Femtosecond to Microsecond Photochemistry of a [FeFe]hydrogenase Enzyme Model Compound

ARTICLE *in* THE JOURNAL OF PHYSICAL CHEMISTRY B · OCTOBER 2010

Impact Factor: 3.3 · DOI: 10.1021/jp107618n · Source: PubMed

8 AUTHORS, INCLUDING:

Stefano Santabarbara
Italian National Research Council
53 PUBLICATIONS **906** CITATIONS

SEE PROFILE

Anthony William Parker
Science and Technology Research Council
412 PUBLICATIONS **6,317** CITATIONS

SEE PROFILE

Christopher Pickett
University of East Anglia
176 PUBLICATIONS **5,669** CITATIONS

SEE PROFILE

Femtosecond to Microsecond Photochemistry of a [FeFe]hydrogenase Enzyme Model Compound

Spyridon Kaziannis,[†] Stefano Santabarbara,[†,⊥] Joseph A. Wright,[‡] Gregory M. Greetham,[§] Michael Towrie,[§] Anthony W. Parker,[§] Christopher J. Pickett,[‡] and Neil T. Hunt*[,†]

Department of Physics, University of Strathclyde, SUPA, 107 Rottenrow East, Glasgow, G4 0NG, U.K.; School of Chemical Sciences, University of East Anglia, Norwich, NR4 7TJ, U.K.; and Central Laser Facility, STFC Rutherford Appleton Laboratory, Didcot, Oxon, OX11 0QX, U.K.

Received: August 12, 2010; Revised Manuscript Received: September 22, 2010

The photochemistry and dynamics of a model compound of the active site of the [FeFe]hydrogenase enzyme system have been studied on a wide range of time scales using a unique combination of femtosecond time-resolved infrared spectroscopy, nanosecond time-resolved infrared spectroscopy, and steady-state UV-FTIR methods. Using three different solvents, heptane, acetonitrile, and cyanoheptane, we have observed the rapid formation of solvent adduct species from the first solvation shell of the solute following photolysis of a carbonyl ligand and global fitting techniques have been employed to provide new insights into the ultrafast dynamics of this process. In addition, the use of solvent mixtures has enabled the observation of competitive ligand substitution processes at the newly created coordination site on time scales of a few nanoseconds, shedding new light on the chemical behavior of these enzyme models.

The hydrogenase family of enzymes plays a biologically important role in anaerobic metabolism through catalysis of the reversible activation of molecular hydrogen. In the case of the [FeFe]hydrogenases, the active site is based upon an Fe_2S_2 cluster with the Fe atoms coordinated by bridging and terminal carbonyl ligands as well as terminal cyano groups.[1,2] The two sulfur atoms are bridged by a short-chain organic link that is thought to include an amino group.[1,2] These species have also generated a significant amount of interest from the synthetic chemistry community where it has been shown that model compounds of the type studied here that derive from the (μ-SRS)$Fe_2(CO)_6$ structural template are also capable of catalyzing the formation of hydrogen.[3] Understanding and control of this process offers the potential to develop novel systems for the production and usage of hydrogen. Furthermore, there exist significant economic benefits in using materials featuring abundant Fe as catalysts for fuel cells as opposed to the precious metals currently in use.

While the macroscopic chemical behavior of these systems has attracted much recent experimental and theoretical interest,[4−11] relatively little is currently known about the reaction mechanism of either the enzyme or the model species. Insights into the transition states formed during the reaction process and the role of the surroundings, in the form of either solvent or the enzyme scaffold, will be crucial in fine-tuning the properties of any technological systems. Studies using irradiation of the CO-inhibited state of the enzyme at cryogenic temperatures have shown evidence for a structure identical to that of the oxidized form and creation of a vacant site in this manner is relevant to understanding of the enzyme process, in which ligand coordination to this vacant site will be a likely first step.[12] Additionally, investigations of model compounds will ultimately allow the roles of active site and protein to be interrogated separately. Work employing ultraviolet activation of model systems in conjunction with Fourier transform infrared (FTIR) spectroscopy have shown that irradiation at wavelengths shorter than 400 nm leads to excitation of a metal to ligand charge transfer (MLCT) transition resulting in the removal of a carbonyl ligand.[13] This has relevance both for the chemistry of the models and the enzyme itself, which rely on the creation of a vacant coordination site at one of the Fe atoms. Studies using ultrafast time-resolved infrared (TRIR) spectroscopy employing a $UV_{pump}-IR_{probe}$ methodology showed the formation of complex photoproduct spectra following irradiation of (μ-$S(CH_2)_3S$)-$Fe_2(CO)_6$ (**1**) in heptane solution at 350 nm.[14] It was suggested that the photoproducts were formed within the time scale on which the system cooled following excitation (~30 ps) but assignment of the photoproduct bands was limited by the complex linear spectrum to a possible mixture of unsaturated pentacarbonyl and solvent adduct species. More recently, density functional theory (DFT)[15] and Raman studies[16] have been used in attempts to shed more light on the photolysis process, while transient 2D-IR (T-2D-IR) methods have used the vibrational coupling patterns and the vibrational dynamics of the photoproduct modes to assign the new species to a single solvent adduct featuring heptane coordinated at the vacant site.[17] It was suggested that the solvent adduct forms from the first solvation shell of the solute and no spectroscopic signature of the unsaturated pentacarbonyl was observed.[17]

Having ascertained the immediate products of photolysis in heptane, which yields excellent spectral resolution by virtue of narrow line widths for vibrational transitions, it is important to extend these studies both to different solvents and to explore the subsequent reactivity of the transient solvent adduct. Here, we present studies of the photolysis of **1** in acetonitrile (MeCN) and 1-cyanoheptane (HeptCN) and compare the results to the established behavior of **1** in heptane solution. Acetonitrile is an important solvent for these model compounds as it has been

* Corresponding author. E-mail: nhunt@phys.strath.ac.uk.
[†] University of Strathclyde.
[‡] University of East Anglia.
[§] STFC Rutherford Appleton Laboratory.
[⊥] Current address: Consiglio Nazionale delle Ricerche, Istituto di Biofisica, Via Celoria 26, 20100 Milano, Italy.

10.1021/jp107618n
Published on Web 10/22/2010

shown that protonation of [FeFe]hydrogenase models, the likely first step in hydrogen formation, occurs readily in MeCN.[18,19] Cyanoheptane provides a useful intermediate between MeCN and heptane by enabling the investigation of mixed solvents (MeCN is immiscible in heptane) where competition reactions between solvent adducts are expected to occur. Such processes will offer insights into subsequent, more complex reactions. By applying several experimental techniques, including femtosecond and ns-TRIR spectroscopy and steady state UV-FTIR methods, covering the range of time scales from femtoseconds to the steady state, we have determined that **1** undergoes rapid formation of a solvent adduct from the first solvation shell in all three solvents and we present for the first time the spectrum of the MeCN and HeptCN adduct species. The use of global fitting procedures sheds new light on the formation rate of the heptane adduct, suggesting that this is somewhat faster than previously shown. Further work in mixed solvents reveals that the heptane adduct undergoes competitive replacement by HeptCN molecules on nanosecond time scales that are heavily dependent upon the concentration of HeptCN.

Experimental Section

The (μ-S(CH$_2$)$_3$S)Fe$_2$(CO)$_6$ (**1**) used in this work was produced using established methods,[3] while the solvents were purchased from Sigma-Aldrich, Ltd., and were used without further purification. Due to the air-sensitive nature of the metal-carbonyl-derivative samples, all solutions were prepared under nitrogen atmosphere and the solvents were purged with dry nitrogen prior to use. The samples were held between CaF_2 windows separated by a 100 μm thickness PTFE spacer, and the concentration of the solutions was optimized to give a peak optical density for the carbonyl stretching vibrational modes in the mid-IR of around 0.5. It was established that the OD at 350 nm was also ~0.5 under these conditions and the concentration of **1** was approximately 1 mM in all experiments. For TRIR studies, the samples were flowed during data collection in order to refresh the sample and prevent build up of photochemical products between laser shots while the sample was rastered in two dimensions perpendicular to the laser beam direction to prevent window damage.

Steady-State UV-FTIR Measurements. FTIR spectra were acquired via a Bruker Vertex 70 FTIR spectrometer modified to allow illumination of the sample by an external source. In this case a 200 W Hg arc lamp, filtered through a combination of a band-pass filter (355 nm central wavelength, 60 nm bandwidth) and a short-frequency pass (cut off 435 nm) filter to remove the visible and short-wavelength components of the spectrum was used for photolysis studies. The UV beam was collimated and focused into the sample and spectra were acquired with a resolution of 0.5 cm^{-1}.

UV_{pump}−IR_{probe} (TRIR) Measurements: fs-TRIR Experiments. The laser system used for fs-TRIR experiments has been described in detail elsewhere.[20] Briefly, the output of a regeneratively amplified Ti:sapphire laser system producing 35 fs duration pulses, centered at 800 nm with a repetition rate of 1 kHz, was used to pump two white light seeded optical parametric amplifiers (OPA). One OPA produced pulses at a wavelength of 350 nm via fourth harmonic generation, which were used as the UV_{pump} pulses. The IR_{probe} pulses originated from the second OPA, which was equipped with difference frequency generation (DFG) to produce tunable mid-infrared radiation. In the present study, the probe pulse was centered at 2000 cm^{-1} with a bandwidth of ~200 cm^{-1} (fwhm), resonant with the CO stretching vibrational modes of **1**.

The time delay between pump and probe pulses was controlled using an optical delay line; this gave a maximum delay time of ~1 ns with a resolution defined by the cross correlation of the pulses of ~300 fs. The relative polarization of the pump and probe pulses was set to the magic angle (54.7°) throughout in order to suppress any contributions from the sample rotational dynamics. For data collection, the pump pulse train was modulated at half the repetition rate of the laser (500 Hz) using an optical chopper and the difference between the spectra of consecutive probe pulses ($UV_{pump\ on} - UV_{pump\ off}$) was recorded as a function of the temporal delay between the pulses. The probe spectrum was measured with a spectrometer and HgCdTe array detector combination.

UV_{pump}−IR_{probe} (TRIR) Measurements: ns-TRIR Experiments. The basic experimental protocol was the same as for the fs-TRIR measurements described above but in this case the IR_{probe} pulses were generated by the ULTRA laser system which has been described previously.[21] In order to reach nanosecond−microsecond pump−probe time delays, the UV_{pump} pulse was produced by a frequency tripled Nd:YAG laser operating at 10 kHz to match the IR_{probe} pulse repetition rate. The pump−probe time delay was determined by a computer-controlled pulse delay generator and the UV_{pump} pulse train modulated at 5 kHz for data collection.

Data Analysis. The data analysis involves the use of a global fitting routine,[22,23] in which the spectral−temporal data matrix ($D(\bar{\nu},t)$) is described by a sum of exponential functions of the form

$$f(\bar{\nu}, t) = \sum_{i}^{n} A_i(\bar{\nu}) \cdot e^{-t/\tau_i} + A_\infty(\bar{\nu}) \qquad (1)$$

where τ_i, the experimental lifetimes, are global parameters, $A_i(\bar{\nu})$ are the decay-associated spectra (DAS), and $A_\infty(\bar{\nu})$ describes processes which do not decay within a given experimental time range (nondecaying or pseudostatic component). The best fit parameters are obtained from minimization of χ^2, where the root-mean-square (rms) noise in the prepump pulse sampling is used as an estimate of the experimental uncertainties in each observation. The minimization routine uses a combination of Simplex (initial parameter search) and Levenberg−Marquardt (optimized search) algorithms to determine the best-fit parameters. The stability of solutions was tested by perturbation of the best fit and the confidence bounds on the best fit parameters are estimated by covariance methods.

Density Functional Theory Simulations. All DFT calculations were carried out using the Gaussian 03 package.[24] Structural optimizations were carried out prior to simulation of infrared spectra. The calculations were performed on gas-phase molecules using the B3LYP functional[25] and the LanL2DZ basis set. The latter employs the Dunning/Huzinaga valence double-ζ D95 V[26] basis set for first-row atoms and the Los Alamos Effective Core Potential plus DZ on atoms from Na−Bi.[27−29] No scaling or correction factors were applied.

Results

Steady-State UV-FTIR of 1. The structure and infrared absorption spectra of **1** in heptane, HeptCN, and MeCN are shown in Figure 1a. The infrared spectrum of **1** dissolved in heptane displays five bands at 1981, 1991, 2006, 2036, and 2075 cm^{-1}, which have been previously assigned to group stretching modes of the Fe$_2$(CO)$_6$ moiety.[20] When **1** is dissolved in MeCN or HeptCN, a pronounced broadening of the lines is observed;

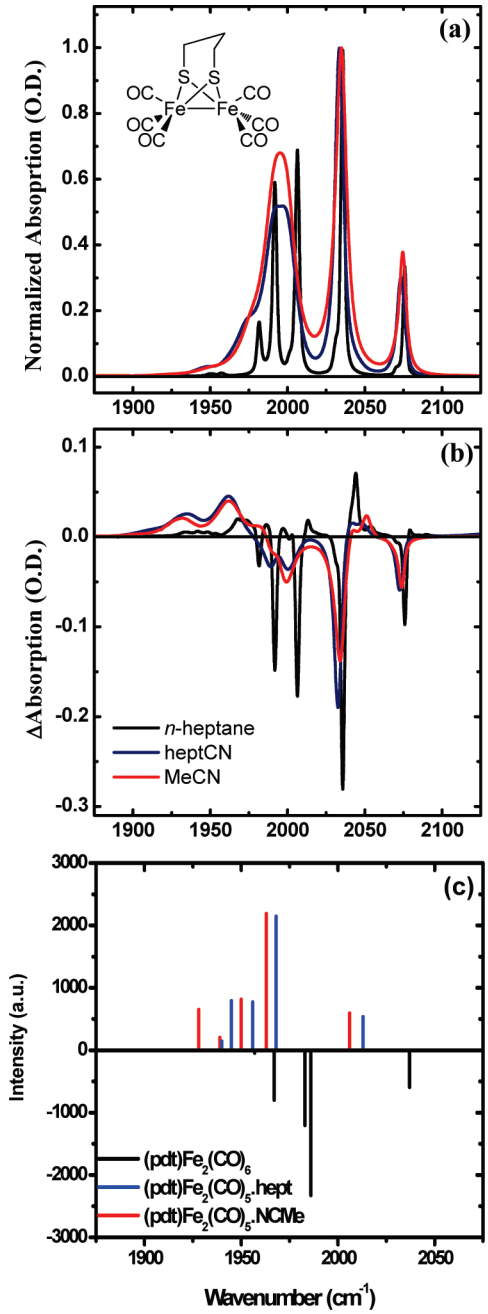

Figure 1. (a) FTIR spectra of **1** dissolved in n-heptane (black), HeptCN (blue), and MeCN (red). The spectra of the neat solvents have been subtracted and the data normalized to the peak at 2035 cm^{-1}. Inset shows structure of **1.** (b) Light minus dark difference FTIR spectra of the samples in (a) recorded after 5 min of continuous UV illumination. (c) DFT-calculated IR spectra of **1** (black), shown as negative peaks for comparison with difference spectra, and that of the *n*-heptane substituted (blue) and MeCN-substituted (red) photoproducts.

the fwhm of the absorption peak at ~2035 cm^{-1} is 2.5, 6.4, and 8.4 cm^{-1} for *n*-heptane, HeptCN, and MeCN, respectively. This leads to the observation of only three bands, located at 1995, 2035, and 2075 cm^{-1} in MeCN and 1997, 2033, and 2073 cm^{-1} in HeptCN. The peaks located at 1995 and 1997 cm^{-1} are particularly broad in these solvents, consistent with this feature arising from the overlap of the three lowest frequency modes of **1**, though the slightly narrower line widths obtained in HeptCN lead to the lowest frequency mode appearing as a shoulder to the broad peak.

Figure 1b shows the UV_{on} minus UV_{off} difference FTIR spectra obtained after 5 min of CW irradiation of solutions of **1** in each of the solvents. In these spectra, negative features indicate the loss of species giving rise to a particular absorption while positive lines indicate the presence of a new species. For **1** in heptane the negative peaks coincide well with the maxima in the absorption spectrum shown in Figure 1a and the positive features are consistent with the photochemical fragmentation of the parent molecule observed previously.[14]

In the case of MeCN and HeptCN, the three negative peaks are again in excellent agreement with the CO stretching modes of the parent species, indicating loss of **1** upon irradiation. In both cases, two relatively broad bands with maxima at ~1930 and ~1960 cm^{-1} are observed along with a third peak near 2052 cm^{-1} for MeCN and 2049 cm^{-1} for HeptCN. Whereas the width and peak position of the photoinduced spectral features are similar in MeCN and HeptCN, the lower frequency modes appear to be 10−20 cm^{-1} down-shifted with respect to those observed in heptane (Figure 1b). This is consistent with the production of a more strongly coordinating solvent adduct such as $(\mu\text{-S(CH}_2)_3\text{S)Fe}_2(\text{CO})_5\cdot$NCR, where R indicates an alkane group. The similarity of the photoproduct spectra obtained for MeCN and HeptCN solutions apparently precludes different binding geometries for the adducts of these two solvents.

In order to confirm this assignment, we performed DFT calculations for $(\mu\text{-S(CH}_2)_3\text{S)Fe}_2(\text{CO})_5\cdot$NCR, where R = Me; it has been shown elsewhere that the length of the alkane chain has little effect on the simulated infrared spectra.[14] The results of these simulations are shown in Figure 1c. As has been discussed elsewhere,[20] in the case of the parent molecule **1**, the calculations predict correctly the general peak pattern and frequency-ordering of the bands but predict less accurately the exact splitting of the CO transitions. Despite this, the replacement of a CO group by a solvent molecule results in the appearance of lower frequency peaks in the calculated spectra, consistent with the experimental results presented above. The down-shift of the lower frequency vibrations is more pronounced in photoproducts involving the CN-substituted solvents than for alkanes. Hence, the outcome of DFT calculations is in general agreement with the results obtained from steady-state UV photolysis, providing further support for the assignment of the newly observed bands to cyanide-linked photoproducts.

fs-TRIR Results. The results obtained for UV-induced photochemistry of **1** in heptane, MeCN, and HeptCN are presented in Figure 2. In the case of **1** in heptane, these show excellent agreement with previously published data.[14] These spectra are included for two reasons: to provide a comparison point for the MeCN and HeptCN results and to provide a control for the results of fitting the new data using a global approach. The results of the global fitting analysis of the data is also shown in Figure 2 (solid lines). A good description of both the dynamics and the spectra recorded at fixed $UV_{pump}-IR_{probe}$ delay times is obtained with three exponential decay time scales alongside a pseudostatic contribution, which does not decay within the investigated time window. A summary of the exponential decays derived by the global fitting procedure is shown in Table 1.

Inspection of the values of the lifetimes (τ_i) obtained from the global analysis indicate that, although differences are observed depending on the specific solvent, a number of common features are also detected. In general, the values of τ_i can be grouped in four time ranges, τ_1 which lies between 7 and 10 ps, τ_2 which occurs in the range 30 to 60 ps, τ_3 which is ~150 ps, and τ_4 which represents the pseudostatic component.

The values obtained for **1** in heptane are consistent with those previously reported from fitting the dynamics of individual

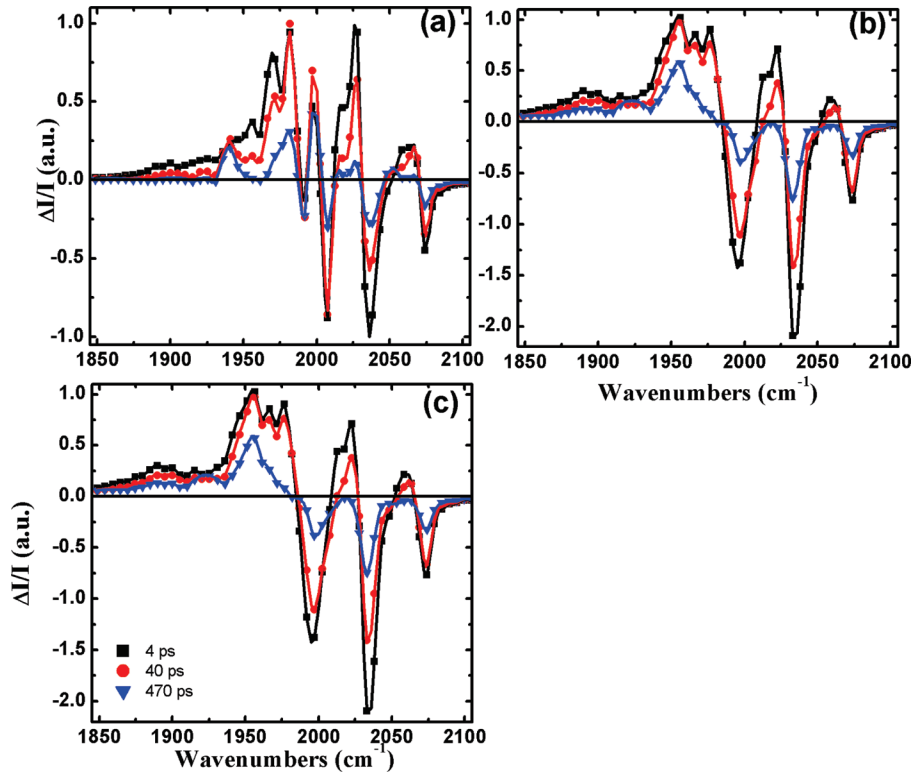

Figure 2. Time-resolved difference fs-TRIR data for **1** dissolved in (a) *n*-heptane, (b) MeCN, and (c) HeptCN at selected pump−probe delay times (symbols). Solid lines are the results of global fitting analysis. All the values are internally normalized to maximal extrapolated intensity of the IR difference spectra at t_0.

TABLE 1: Decay Constants of the Three Exponential Decay Time Scales Obtained via a Global Fitting Analysis of fs-TRIR Spectra

	τ_1 (ps)	τ_2 (ps)	τ_3 (ps)
n-heptane	7 ± 2	30 ± 5	156 ± 15
MeCN	10 ± 3	60 ± 7	142 ± 15
heptCN	7 ± 2	49 ± 7	147 ± 15

peaks. The latter approach resulted in three dynamical components: a broadband contribution attributed to vibrational cooling with a time scale of 30 ps, which coincided with the appearance of the photoproduct peaks; a 150 ps decay of the parent bleach signals that was attributed to geminate recombination of the pentacarbonyl and CO ligand to reform the parent molecule; and a several nanosecond decay time scale corresponding to loss of the metastable photoproduct. Using the global approach returned time scales of 7, 30, and 150 ps, alongside a pseudostatic component, which are in excellent agreement and confirm the validity of the global approach.[14] That the faster of these decay lifetimes (τ_1) was not resolved in the previous investigation is due to an increased time resolution of the spectrometer and the acquisition of a greater number of data points near the zero pump−probe time delay. Similarly, the global analysis returns a pseudostatic paramenter in place of the several nanosecond decay time from previous work.

In the case of **1** in MeCN and HeptCN, the spectra obtained are broadly similar both to each other and to those observed via FTIR experiments. While the peak positions are similar, the relative peak intensities show some variation between the Me and Hept derivatives, though this may be partially due to the lower resolution and signal-to-noise ratios obtainable in the fs-TRIR experiments versus UV-FTIR measurements. It is also noticeable that the spectra contrast with the data obtained for the heptane sample in that the photoproduct peaks are shifted to lower frequency in comparison to those observed for the heptane sample, as would be consistent with formation of a CN substituted solvent adduct (Figure 1c).

From the global fitting, it appears that the value of τ_2 (30−60 ps) displays the most pronounced dependence on the nature of the solvent, whereas the value of τ_1 (7−10 ps) and τ_3 (∼150 ps) are almost solvent-independent within the accuracy of the experiment. This is broadly consistent with τ_3 being assigned to geminate recombination while the solvent dependence of τ_2 is likely to be due to the differing abilities of the solvents to mediate vibrational relaxation.

More detailed information can be gleaned from the global fitting approach via the decay associated spectra (DAS) for each of the decay time scales. In principle, the DAS provide information relating to the chemical species and the photochemical processes associated with each decay lifetime. Figure 3 shows the DAS determined for **1** in the three different solvents, whereas a comparison of the initial difference IR spectra, i.e., extrapolation to t_0 (zero pump−probe time delay), and the final spectra, i.e., the pseudostatic component, are shown in Figure 4.

The DAS associated with the lifetime of 7−10 ps (Figure 3a) show significant amplitude only in the portion of the spectrum overlapped with ground-state absorption, i.e., $\upsilon > 1950$ cm^{-1}. Thus, this rapid process does not appear to be associated with the formation of solvent adducts as these species would display transitions in the lower frequency region of the spectrum. One possible assignment could be to the electronically excited state of **1** and its associated relaxation to the ground state without dissociation. The rapid loss of this species would be consistent with it not being observed either by previous TRIR analysis not employing global approaches or the lower time resolution T-2D-IR methods.[17]

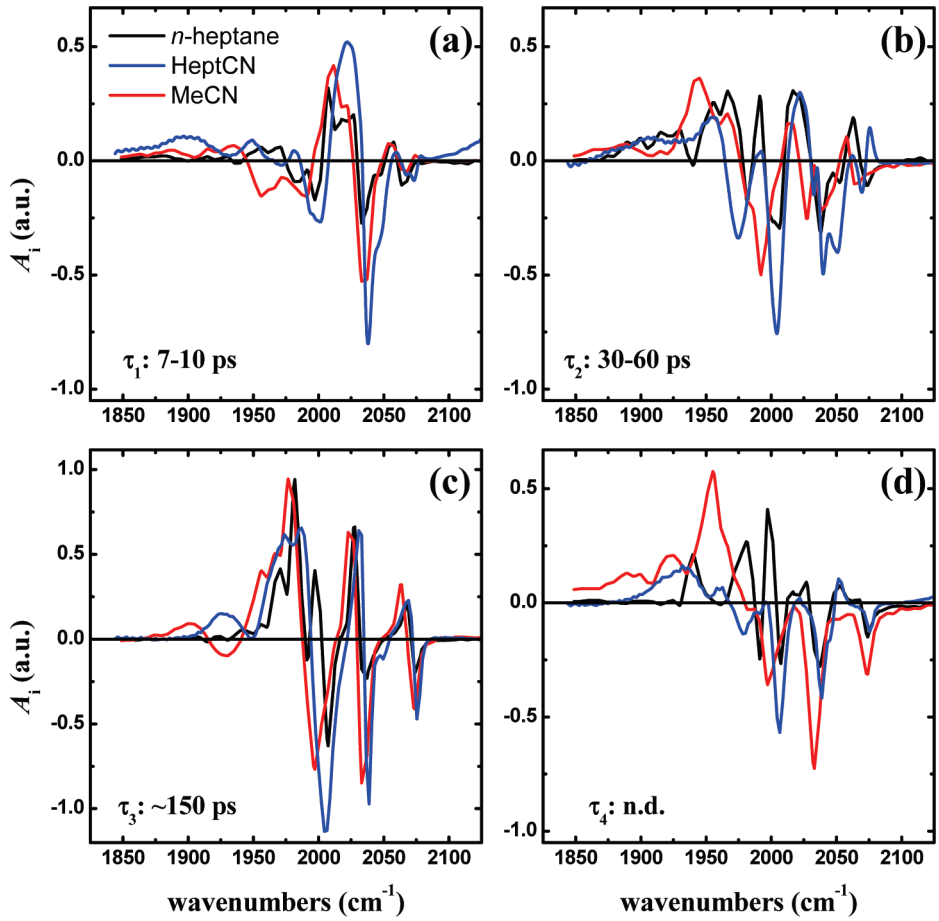

Figure 3. Decay-associated spectra (DAS) obtained from global fitting of TRIR experiments for **1** dissolved in *n*-heptane (black), HeptCN (blue), and MeCN (red): DAS of (a) $\tau_1 \sim 7-10$ ps; (b) $\tau_2 \sim 30-60$ ps; (c) $\tau_3 \sim 150$ ps; and (d) τ_4 pseudostatic component. All DAS are internally normalized on the maximum (positive) amplitude of the spectra extrapolated to t_0 (Figure 4).

The DAS of the two faster lifetimes, particularly the 30−60 ps component, display relatively broad features with respect to both the steady-state absorption and the DAS of the slower components. The DAS associated with $\tau_2 \sim 30-60$ ps (Figure 3b) contains similar spectral features for each of the three solvents, though some peak positions are shifted in frequency in MeCN and HeptCN solutions and are less obvious due to the effects of line broadening. In all cases, the positions of the bleaches coincide with parent molecule absorption peaks, whereas the associated absorptions are red-shifted by 5−15 cm^{-1}. These spectral patterns are consistent with a process involving relaxation of vibrationally excited states, which are shifted by the effects of the anharmonicity of the vibrational modes. The appearance of low-frequency modes (<1950 cm^{-1}) may also indicate solvent adduct involvement and it is noteworthy that the time scales reported are similar in magnitude to the 65 ± 10 ps vibrational relaxation time (T_1) of the heptane adduct observed by T-2D-IR methods.[17]

The DAS associated with τ_3, i.e., the 150 ps lifetime (Figure 3c), display a complex spectral pattern showing pairs of transitions which, coincide well with the parent molecule υ_{0-1} vibrational modes and the accompanying υ_{1-2} transitions.[20] This general trend is repeated for the data in MeCN and HeptCN. Overall, the line widths of these transitions are narrower in the 150 ps DAS in comparison with the faster decay time scales. Indeed, they are more comparable to those recorded in the steady-state FTIR measurements indicating that excited electronic state contributions are negligible and suggesting the most likely assignment, as also concluded previously,[14] is the recombination of CO and the pentacarbonyl molecular fragment to reform the parent molecule. The presence of the positive peaks is thus attributed to the transient absorption from the first excited CO vibrational levels of the parent molecule. The positions are consistent with observed values for the anharmonicity of **1** and these levels can be populated through relaxation following recombination. The time scales are also consistent with the solvent independent T_1 times observed via 2D-IR spectroscopy of **1**.[20] The positions of the decaying positive peaks at 2069, 2028, 1998, and 1981 cm^{-1} are also in agreement with DFT calculation predictions of a down-shift of carbonyl stretching modes in the unsaturated pentacarbonyl species,[14] which would also be consistent with geminate recombination.

Finally, it is instructive to compare the DAS of the pseudostatic component with the long time delay experimental TRIR data and the extrapolated t_0 spectra; these are shown in Figure 4. As mentioned earlier, the pseudostatic DAS describes a spectral contribution that is not decaying within the range of the experimental pump−probe delay time. It is evident for all the solvents used that the DAS of the pseudostatic component is identical, within experimental error, to the spectra recorded at the longest time delays. This is emphasized for the case of *n*-heptane in the inset of Figure 4a. For MeCN and HeptCN, the DAS of the pseudostatic components also shows a strong similarity in terms of peak positions to the UV-FTIR difference spectra (Figure 1b). Small differences are observed in heptane solutions that will be discussed below. The most distinctive photoproduct features are the positive bands in the 1850−1975 cm^{-1} region, which are attributable to the formation of solvent

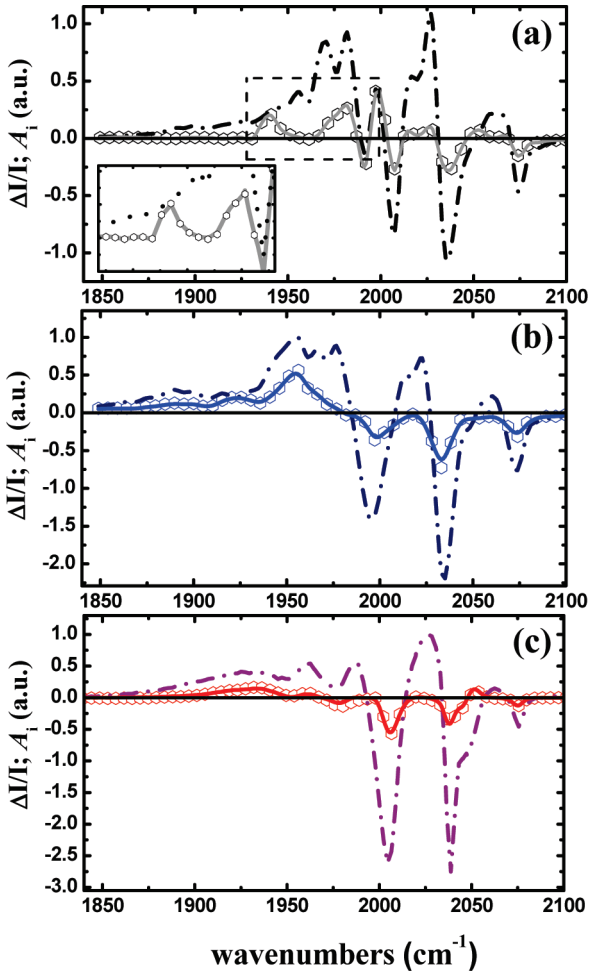

Figure 4. Comparison of the fs-TRIR spectra extrapolated to t_0 from the global fit (dashed-dotted lines), the DAS of the nondecaying components (solid lines) and the experimental fs-TRIR spectra recorded at the longest experimental $UV_{pump}-IR_{probe}$ delay (open symbols), in (a) *n*-heptane, (b) MeCN, and (c) HeptCN. The spectra are internally normalized to the maximum value of t_0.

adducts. Above 1975 cm^{-1}, the DAS of the pseudostatic contribution is dominated by the parent molecule bleaches for all three solvents. Moreover, the comparison of the nondecaying spectra with that of initial photolysis (t_0) suggests that the substitution of a carbonyl ligand with a solvent molecule takes place at very short times. This is, for instance, particularly evident for the 1941 cm^{-1} peak of the heptane adduct, as the nondecaying component contributes, essentially, the entire amplitude to t_0 (Figure 4a). In previous studies, the observation of photoproduct peaks coincided with the loss of signatures due to local heating. The use of global fitting separates these contributions and suggests that the formation process is somewhat faster than previously described.[14]

ns-TRIR Results. In the case of solutions of **1** in MeCN and HeptCN, little difference was noted between the UV-FTIR data and the pseudostatic spectral component observed in the fs-TRIR data. As such, it can be assumed that no photochemistry occurs in the intervening period. This was not the case in solutions of heptane, however, with peaks appearing in the UV-FTIR spectra that were not present in the pseudostatic fs-TRIR component. Similarly, fs-TRIR experiments in which **1** was photolyzed in a solvent mixture of HeptCN and heptane (MeCN is immiscible in heptane) showed that the pseudostatic component corresponded to the spectrum of the solvent adduct of the solvent species present in the greatest fraction, while UV-FTIR data indicated that the HeptCN adduct was always the most stable at longer delay times. The implication of these observations was that the heptane adduct undergoes competitive substitution in favor of the more stable HeptCN adduct on time scales greater than 1 ns. To study these processes further, ns-TRIR experiments were carried out on both **1** in heptane and **1** in solvent mixtures of heptane and HeptCN.

Figure 5a shows the ns-TRIR dynamics for **1** dissolved in *n*-heptane. As for the ultrafast time scale, the data were analyzed using a global procedure. In this case, the dynamics were much more straightforward since there is no contribution from vibrational cooling on these time scales. The data were well described by the sum of a single-exponential decay ($\tau = 330$ ns) and a pseudostatic component. Figure 5b shows the temporal dynamics of some of the peaks observed, and the DAS retrieved from the global analysis are shown Figure 5c, together with the extrapolated initial spectrum, which in this case corresponds to the difference spectrum at 3 ns delay following photolysis (t_{3n}).

In order to facilitate a direct comparison of the spectral features observed at different time scales for **1** in heptane, Table 2 provides a summary of the peak positions as they appear in the pseudostatic component of the fs-TRIR experiments, the initial (t_{3n}) and pseudostatic DAS of the ns-TRIR data and the UV-FTIR difference spectrum. The pseudostatic DAS of the fs-TRIR data and the extrapolated initial ns-TRIR spectrum display the same spectral features, indicating that there is no substantial spectral evolution in the time window (1−3 ns) not explicitly covered by experiment. The peaks observed in the DAS of the pseudostatic ns-TRIR component are in excellent agreement with the steady-state UV-FTIR spectrum but the majority of these peaks are not observed in the t_{3n}-extrapolated spectra (Figure 5c). These observations indicate that the photoproduct formed during the fs-TRIR experiment is converted on nanosecond time scales into the species observed under steady-state conditions.

The 330 ns DAS displays positive peaks at ∼1977, 1997, and 2051 cm^{-1} and negative ones at 1960−1970, 2015, 2044, and 2054 cm^{-1}. Comparison with the time traces (Figure 5b) alongside the mirror image relationship of DAS corresponding to the ns-TRIR pseudostatic component and the 330 ns component confirms that this process describes interconversion of the initial species present at ∼1 ns, absorbing at 1977, 1997, and 2051 cm^{-1}, into another absorbing at 1960−1970, 2015, 2044, and 2054 cm^{-1}, observed under steady-state conditions. The identity of this final species in the neat *n*-heptane solvent is unclear though possible candidates will be discussed below.

Photolysis of **1** was also carried out in mixtures of HeptCN and heptane. The concentration of HeptCN was varied between 20 and 740 mM, allowing a range of molecular ratios between the solute (**1**, 1 mM), the "reactant" species HeptCN and the bulk solvent (*n*-heptane, 6.8 M) to be explored.

The resulting dynamics are shown most clearly by the characteristic absorptions of the heptane adduct at 1978 cm^{-1} and the HeptCN adduct at 1959 cm^{-1}. These are shown in Figure 6a, together with the results of the global fitting procedure and the DAS for two particular concentrations of HeptCN (100 and 340 mM) in *n*-heptane Figure 6b,c. These two diagnostic peaks clearly have opposing dynamics indicating interconversion between these species. This is also clear from comparing the data in the t_0 and the pseudostatic DAS (Figure 6b,c).

The $UV_{pump}-IR_{probe}$ time delay at which this interconversion occurred became shorter as the concentration of HeptCN increased, as would be expected. The best global fits, at all

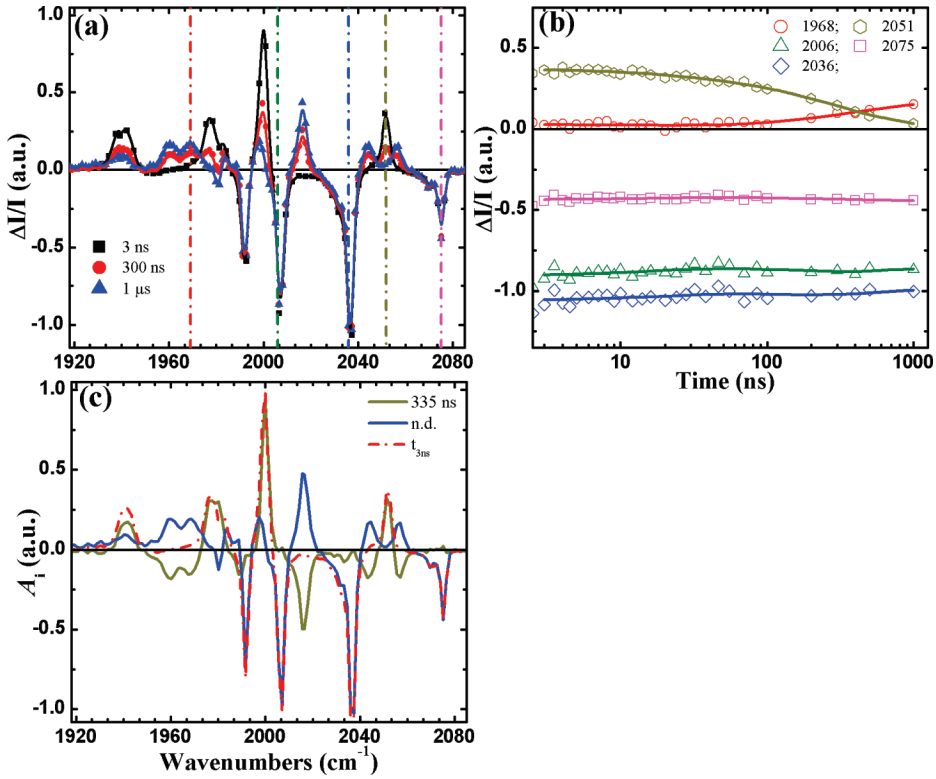

Figure 5. ns-TRIR results for **1** dissolved in *n*-heptane. (a) TRIR spectra at selected time delays. The color-coded lines indicate the spectral positions for which the dynamics are presented in panel (b). The solid lines in panels (a) and (b) are the best fits resulting from the global analysis of the experimental data. (c) Decay-associated spectra (DAS) resulting from the global fitting of the kinetics for the 330 ns component, nondecaying component, and the extrapolated initial spectrum (t_{3n}). All the values are internally normalized on the maximum value of t_{3n}.

TABLE 2: Peaks Positions (cm^{-1}) Observed in DAS Components of the ns-TRIR and fs-TRIR Data and the UV-FTIR Spectra for 1 in *n*-Heptane

		ns-TRIR		
	fs-TRIR pseudostatic	t_{3n}	pseudostatic	UV-FTIR
bleaches (cm^{-1})	—[a]	—[a]	1980	1982
	1991	1991	1991	1992
	2007	2007	2007	2006
	2036	2036	2036	2036
	2075	2075	2075	2076
photoproduct absorptions (cm^{-1})	1941	1941	1940	1933−1948
	—	—	1960−1970	1965−1973
	1980	1976−1981	—	—
	1997	1999	1997	1997
	—	—	2015	2013
	—	—	2044	2044
	2052	2052	—	—
	—	—	2055	2054

[a] Peaks are not observed due to overlap with the positive photoproduct peak at 1976−1981 cm^{-1}. * The spectral resolution is 4, 1, 0.5 cm^{-1} for the ps-TRIR, ns-TRIR, and FTIR, respectively.

concentrations of HeptCN, were obtained using two exponential decay time scales, one in the 4−30 ns range, another in the ∼330−350 ns, as well as a pseudostatic component. The value of the major component (4−30 ns) of the fit, attributable to the interconversion time via the DAS (Figure 6b,c), displayed a lifetime that was heavily dependent upon the concentration of HeptCN, decreasing with increasing concentration of HeptCN. The DAS of these fast components were identical for all HeptCN concentrations, suggesting that they are attributable to the same process. The amplitude of the 330−350 ns lifetime component was small, less than 3−5% of the amplitude of $t_{3\,ns}$ after photolysis. Because of the similarity of this lifetime with the principal decay component observed in neat *n*-heptane solution, this process is attributed to the same chemical reaction as was observed in neat heptane. The value of this lifetime was virtually independent of the concentration of HeptCN as would be expected.

The dependence of the rate of formation of HeptCN adduct as a function of the initial HeptCN concentration is shown in Figure 7a. Using the reasonable assumption that the experimental lifetimes represent the inverse of the reaction rate constants, the latter display an almost linear dependence on the concentration of HeptCN in the solvent mixture, as expected for a diffusion-controlled reaction (Figure 7b). A linear regression analysis of the rate dependence as a function of HeptCN concentration, forced through the origin for vanishing concentration of HeptCN, yielded bimolecular rate constants of 4.25×10^8 s^{-1} M^{-1}.

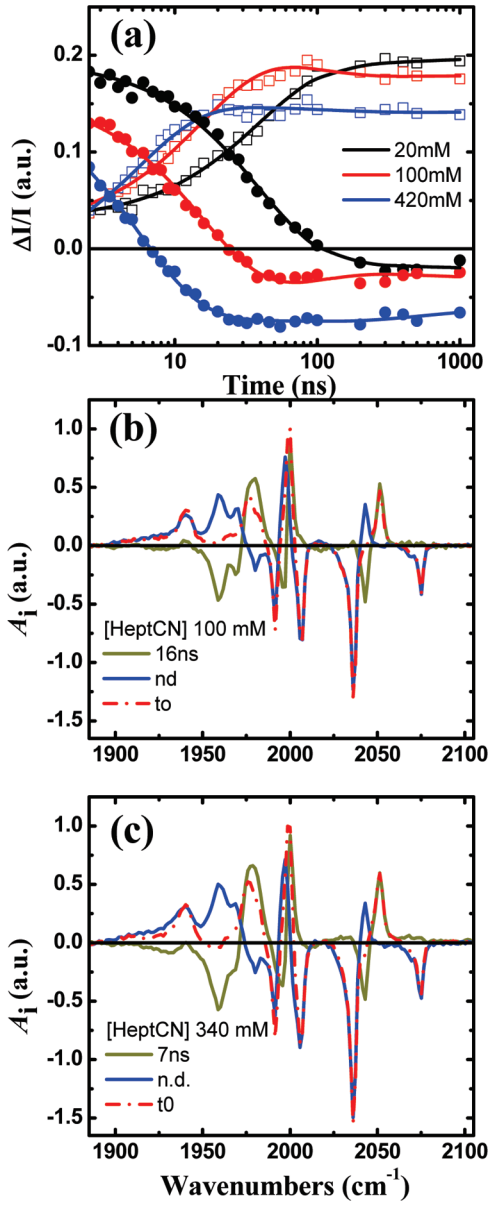

Figure 6. (a) Dynamics in the nanosecond-to-microsecond time scale of UV-induced photochemistry of **1** dissolved in mixtures of heptane/HeptCN, monitored at 1959 cm^{-1} (□) and 1978 cm^{-1} (●). The solid lines are the global fits to the kinetic traces. (b,c) Decay-associated spectra (DAS) of **1** in the nanosecond-to-microsecond time window, acquired in two mixtures of heptane/HeptCN: (b) 100 mM HeptCN and (c) 340 mM HeptCN. Gold solid lines, principal component DAS; blue solid lines, nondecaying DAS; red dash-dotted lines, extrapolation to $t_{3\,ns}$. The low-amplitude 330 ns DAS is omitted for clarity. The spectra are internally normalized on the maximum value of t_{3n}.

Discussion

In summary, the fs-TRIR data show that photolysis of **1** in MeCN and HeptCN results in the rapid formation of a new species. DFT simulations and comparisons with TRIR,[14] 2D-IR,[20] and T-2D-IR studies of **1** in heptane[17] enable assignment of this to a solvent adduct. The picosecond dynamics in all solvents are similar, revealing excited-state relaxation processes on 7−10 ps time scales and vibrational cooling on 30−60 ps time scales. A ∼150 ps process is also resolved and ascribed to geminate recombination and parent molecule vibrational relaxation, which are not individually resolved as they occur on similar time scales. Global analysis suggests that CO loss and solvent adduct formation occurs on a subpicosecond time scale while the solvent adduct is observed to remain beyond the 1 ns time window of this experiment, indicating a metastable nature. Indeed, in the CN-substituted solvents, the similarities between the pseudostatic fs-TRIR data and the UV-FTIR data indicate that these species are stable to significantly longer times. These results are summarized in Figure 8.

The dynamics of the UV-induced photochemistry of **1** in different solvents have been investigated over a broad temporal window ranging from femtoseconds to microseconds following UV irradiation, as well as under steady-state conditions. We have observed complex kinetic behavior including competitive substitution of solvent adducts extending throughout the investigated time range.

UV irradiation of dimetallocarbonyl complexes is known to yield two principal products; the homolytic breaking of the intermetallic bond, and the dissociation of a carbonyl group.[13] The relative populations of the two possible product species are dependent upon the excitation wavelength with shorter wavelengths tending to favor the MLCT transition that leads to carbonyl cleavage.[13,30−32] Since in **1** the two iron atoms are held in a relatively rigid geometry due to the bridging disulfide moiety, cleavage of the Fe−Fe bond does not give rise to molecular fragments; rather extremely fast geminate recombination to the parent molecule would be expected to take place. However, in unbridged dithiolate species, evidence for formation of an isomeric form has been reported upon Fe−Fe bond cleavage in Nujol mulls.[13]

The breaking of the Fe−CO bond is not restricted by the molecular architecture, however, so dissociation of a CO ligand is accompanied by formation of CO-depleted parent molecule. The data suggest that these molecular fragments undergo recombination to the parent molecule in 150 ps provided that the CO ligand does not escape from the solvent cage. The lifetime associated with this particular process appears to be independent of the chemical nature of the bulk solvent, despite differences in the molecular sizes, which range from 41 (MeCN) to 113 g mol^{-1} (HeptCN) and viscosities (MeCN = 0.369; HeptCN = 0.813 cP)[33] of the solvents, properties that both affect the diffusion coefficient. The absence of any significant dependence of the rate of recombination from the macroscopic properties of bulk solvents is thus supportive of intrasolvent cage recombination. It seems reasonable that the relatively long time scale for bleach recovery is linked to the ground-state vibrational relaxation time of **1**, which has also been shown to be solvent independent.[20]

The results presented above also indicate that an alternative reaction path competes with molecular recombination: that of replacement of the photolyzed CO ligand with a solvent molecule. Despite being able to resolve dynamic process with time constants as fast as 7−10 ps, none of the spectra associated with these time scales show clear evidence for the formation of products other than the solvent adduct, irrespective of the solvent used. This also strongly suggests that this quasi-instantaneous formation of the solvent photoproduct occurs from within the first solvation sphere.

Excluding the very rapid formation of the solvent adduct and geminate recombination, we do not observe any other evidence for chemical reaction in the subnanosecond time scale, neither in neat solvents nor in solvent mixtures, even at very elevated HeptCN concentrations. Rather, the dynamic processes occurring appear to be associated with relaxation of vibrationally excited states of the parent molecule, the molecular fragments, and the solvent adducts. The lifetimes attributed to these photophysical processes are in general agreement with those reported from

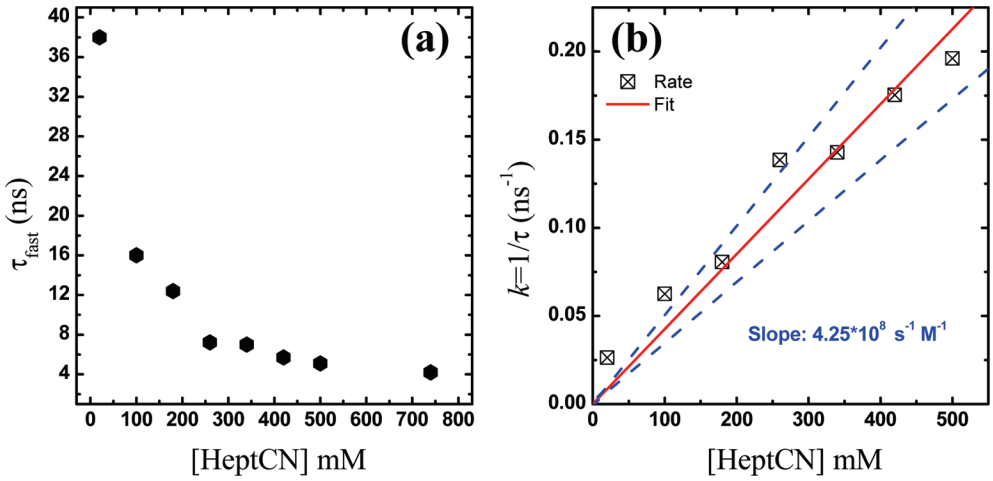

Figure 7. (a) Dependence of the 4−30 ps time scale component upon HeptCN concentration derived from global fitting of ns-TRIR data. (b) Dependence of the reaction rate for interconversion of the solvent adducts ($k = \tau^{-1}$) as a function of the concentration of HeptCN and linear regression expected for a bimolecular process. Solid red line, best fit through the origin; dashed blue lines, confidence interval ($p = 0.9$).

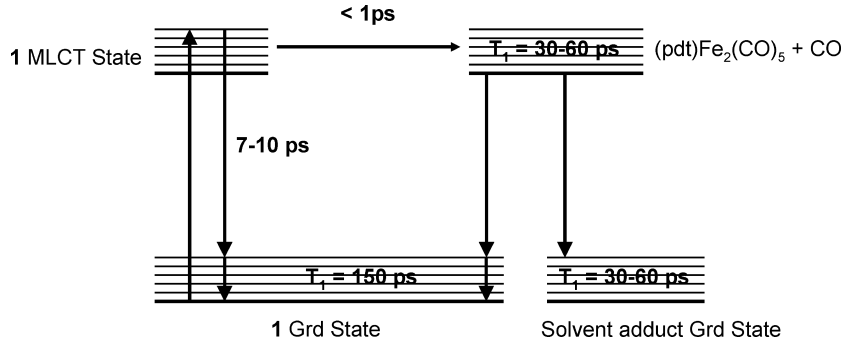

Figure 8. Diagram summarizing processes and time scales following excitation of **1** at 350 nm. T_1 indicates vibrational relaxation time scales.

2D-IR experiments, which probe vibrational dynamics of the parent molecule **1** in the ground electronic state[20] and T-2D-IR studies of the heptane solvent adduct.[17]

The observation of further chemical processes on the nanosecond time scale in both neat heptane and mixtures of heptane and HeptCN is extremely interesting and relevant to further studies of these model compounds. The appearance of these bands is correlated to the disappearance of molecular species generated during the fs-TRIR experiments. The processes does not involve the recovery or further breakdown of the parent molecule, as the peaks originating from the bleaching of absorptions due to **1** display little dynamic behavior in this time range. In mixed solvents, the position of the new transitions appearing in the 4−30 ns time interval are consistent with substitution of heptane by HeptCN. This implies that the adduct formed on the ultrafast time scale is a metastable species, rather than a highly reactive unsaturated species. Moreover, in solvent mixtures the relationship between the appearance time scales of these bands and the concentration of HeptCN is consistent with bimolecular kinetics (Figure 7), pointing toward a diffusion limited reaction. However, increasing the concentration of HeptCN does not lead to a continued increase in the reaction rate; rather, the rate increases until such concentration as HeptCN becomes part of the first solvation shell, whereupon fs-TRIR experiments in mixtures indicate that the HeptCN adduct is formed preferentially as would be expected.

When strongly coordinating species are present in the solvent mixture, they kinetically outcompete the chemical process that occurs in neat heptane on 300 ns time scales. In neat heptane, we again observed no recovery of the parent molecule bleaches, but significant shifts in the frequencies of photoproduct carbonyl modes were observed. This seems to indicate a reconfiguration of the initial photoproducts. It is known that the agostic interactions are relatively stable.[34] However, drawing electron density from the alkane chain to the metal center increases the acidity of the hydrogen atom involved in the bond.[35] This in turn can lead to elimination to yield a direct metal−carbon bond.

An alternative candidate for the new peaks observed in heptane solution at the longest of times following activation is the formation of a pseudodimeric species. Given the concentrations present, this would seem more likely between a solvent adduct and an unreacted parent molecule, as opposed to dimerization of two solvent adducts. The low concentrations of these species present would correlate with the long appearance time scale for this new species, however, and the increased number of photoproduct bands would also be in good agreement with a structurally complex species. Reaction with remaining parent molecules is not consistent with the lack of temporal evolution of the parent bleaches, but the low expected relative changes in concentration may not be detectable. In this case, a CO-bridged species may be anticipated though no evidence for a bridging CO mode was observed in any of the experiments described above.

Conclusions

In summary, we have employed UV_{pump}−IR_{probe} spectroscopies to observe the photolysis and subsequent photochemistry of a model compound of the hydrogenase enzyme system over a wide range of time scales. This work has determined that UV photolysis of **1** in heptane, HeptCN, or MeCN promotes

the substitution of a carbonyl ligand with a solvent molecule, giving rise to a metastable solvent adduct, irrespective of the solvent studied. This is an ultrafast process occurring on the order of a few picoseconds, implying that the participating molecules are part of the solvation sphere. Moreover, the dynamics of the ultrafast solvent adduct formation are largely independent of the nature of the solvent.

Second, we have observed photochemistry of the heptane solvent adduct in mixed solvents in which a diffusion-limited process is observed when a more strongly coordinating molecule is present in a minority concentration. This occurs in the tens of nanoseconds time scale ($4\ \text{ns} < \tau < 30\ \text{ns}$) with a bimolecular reaction rate constant of $k_{ex} = 4.25 \times 10^8\ \text{s}^{-1}\ \text{M}^{-1}$ and is assigned to the exchange of the solvent adduct ligand from heptane to the more thermodynamically stable HeptCN.

We believe that this study provides a basis for further investigations of these important complexes that lie outside the scope of this article. In particular, a study of the nitrile stretching vibrational mode would provide an alternative viewpoint for the solvent coordination process. Evidence for changes in this mode were observed as would be expected, but as it was not consistently accessible by all of the experiments used here due to differing laser pulse bandwidths, this has not been included in the discussion. Other interesting directions might include isotopic labeling of the reactants to assist with assignment, though previous studies show excellent agreement between experiment and theory for the parent hexacarbonyl species.[20] Extension of the study to other ligands would also be interesting and work is underway in this area. Of particular relevance to enzyme studies would be studies in the presence of an H^+ source and stop-flow studies have already indicated that protonation of model species proceeds under acidic conditions.[18]

Acknowledgment. The authors acknowledge funding for this work from EPSRC (UK) for an Advanced Research Fellowship (N.T.H.), from the European Research Council for a Starting Investigator Grant (N.T.H., S.K., S.S.), and from STFC (UK) for a Programme Access Grant (N.T.H.). J.A.W. acknowledges funding from the BBSRC (UK).

References and Notes

(1) Nicolet, Y.; Piras, C.; Legrand, P.; Hatchikian, C. E.; Fontecilla-Camps, J. C. *Struct. Folding Des.* **1999**, *7*, 13.

(2) Nicolet, Y.; Cavazza, C.; Fontecilla-Camps, J. C. *J. Inorg. Biochem.* **2002**, *91*, 1.

(3) Liu, X. M.; Ibrahim, S. K.; Tard, C.; Pickett, C. J. *Coord. Chem. Rev.* **2005**, *249*, 1641.

(4) Barton, B. E.; Olsen, M. T.; Rauchfuss, T. B. *Curr. Opin. Biotechnol.* **2010**, *21*, 232.

(5) Orain, P. Y.; Capon, J. F.; Gloaguen, F.; Petillon, F. Y.; Schollhammer, P.; Talarmin, J.; Zampella, G.; De Gioia, L.; Roisnel, T. *Inorg. Chem.* **2010**, *49*, 5003.

(6) Bertini, L.; Greco, C.; Bruschi, M.; Fantucci, P.; De Gioia, L. *Organometallics* **2010**, *29*, 2013.

(7) Song, L. C.; Li, Q. S.; Yang, Z. Y.; Hua, Y. J.; Bian, H. Z.; Hu, Q. M. *Eur. J. Inorg. Chem.* **2010**, *7*, 1119.

(8) Jablonskyte, A.; Wright, J. A.; Pickett, C. J. *Dalton Trans.* **2010**, *39*, 3026.

(9) Salomone-Stagni, M.; Stellato, F.; Whaley, C. M.; Vogt, S.; Morante, S.; Shima, S.; Rauchfuss, T. B.; Meyer-Klaucke, W. *Dalton Trans.* **2010**, *39*, 3057.

(10) George, S. J.; Cui, Z.; Razavet, M.; Pickett, C. J. *Chem.—Eur. J.* **2002**, *8*, 4037.

(11) Tard, C.; Pickett, C. J. *Chem. Rev.* **2009**, *109*, 2245.

(12) Chen, Z.; Lemon, B. J.; Huang, S.; Swartz, D. J.; Peters, J. W.; Bagley, K. A. *Biochemistry* **2002**, *41*, 2036.

(13) Silaghi-Dumitrescu, I.; Bitterwolf, T. E.; King, R. B. *J. Am. Chem. Soc.* **2006**, *128*, 5342.

(14) Ridley, A. R.; Stewart, A. I.; Adamczyk, K.; Ghosh, H. N.; Kerkeni, B.; Guo, Z. X.; Nibbering, E. T. J.; Pickett, C. J.; Hunt, N. T. *Inorg. Chem.* **2008**, *47*, 7453.

(15) Bertini, L.; Greco, C.; de Gioia, L.; Fantucci, P. *J. Phys. Chem. A* **2009**, *113*, 5657.

(16) Galinato, M. G. I.; Whaley, C. M.; Lehnert, N. *Inorg. Chem.* **2010**, *49*, 3201.

(17) Stewart, A. I.; Wright, J. A.; Greetham, G. M.; Kaziannis, S.; Santabarbara, S.; Towrie, M.; Parker, A. W.; Pickett, C. J.; Hunt, N. T. *Inorg. Chem.* **2010**, *49*, 9563−9573.

(18) Wright, J. A.; Pickett, C. J. *Chem. Commun.* **2009**, *38*, 5719.

(19) Capon, J. F.; Ezzaher, S.; Gloaguen, F.; Petillon, F. Y.; Schollhammer, P.; Talarmin, J. *Chem.—Eur. J.* **2008**, *14*, 1954.

(20) Stewart, A. I.; Clark, I. P.; Towrie, M.; Ibrahim, S.; Parker, A. W.; Pickett, C. J.; Hunt, N. T. *J. Phys. Chem. B* **2008**, *112*, 10023.

(21) Kania, R.; Stewart, A. I.; Clark, I. P.; Greetham, G. M.; Parker, A. W.; Towrie, M.; Hunt, N. T. *Phys. Chem. Chem. Phys.* **2010**, *12*, 1051.

(22) Beechem, J. M. *Methods Enzymol.* **1992**, *210*, 37.

(23) van Stokkum, I. H.; Larsen, D. S.; van Grondelle, R. *Biochim. Biophys. Acta* **2004**, *1657*, 82.

(24) Frisch, M. J.; Trucks, G. W.; Schlegel, H. B.; Scuseria, G. E.; Robb, M. A.; Cheeseman, J. R.; Jr., J. A. M.; Vreven, T.; Kudin, K. N.; Burant, J. C.; Millam, J. M.; Iyengar, S. S.; Tomasi, J.; Barone, V.; Mennucci, B.; Cossi, M.; Scalmani, G.; Rega, N.; Petersson, G. A.; Nakatsuji, H.; Hada, M.; Ehara, M.; Toyota, K.; Fukuda, R.; Hasegawa, J.; Ishida, M.; Nakajima, T.; Honda, Y.; Kitao, O.; Nakai, H.; Klene, M.; Li, X.; Knox, J. E.; Hratchian, H. P.; Cross, J. B.; Bakken, V.; Adamo, C.; Jaramillo, J.; Gomperts, R.; Stratmann, R. E.; Yazyev, O.; Austin, A. J.; Cammi, R.; Pomelli, C.; Ochterski, J. W.; Ayala, P. Y.; Morokuma, K.; Voth, G. A.; Salvador, P.; Dannenberg, J. J.; Zakrzewski, V. G.; Dapprich, S.; Daniels, A. D.; Strain, M. C.; Farkas, O.; Malick, D. K.; Rabuck, A. D.; Raghavachari, K.; Foresman, J. B.; Ortiz, J. V.; Cui, Q.; Baboul, A. G.; Clifford, S.; Cioslowski, J.; Stefanov, B. B.; Liu, G.; Liashenko, A.; Piskorz, P.; Komaromi, I.; Martin, R. L.; Fox, D. J.; Keith, T.; Al-Laham, M. A.; Peng, C. Y.; Nanayakkara, A.; Challacombe, M.; Gill, P. M. W.; Johnson, B.; Chen, W.; Wong, M. W.; Gonzalez, C.; Pople, J. A. *Gaussian 03, Revision C.01*; Gaussian, Inc: Wallingford, CT, 2004.

(25) Stephens, P. J.; Devlin, F. J.; Chabalowski, C. F.; Frisch, M. J. Ab initio calculation of vibrational absorption and circular dichroism spectra using density functional force fields. *J. Phys. Chem.* **1994**, *98*, 11623–11627. Hertwig, R. H.; Koch, W. On the parameterization of the local correlation functional: What is Becke-3-LYP. *Chem. Phys. Lett.* **1997**, *268*, 345–351.

(26) Dunning Jr., T. H.; Hay, P. J. *Modern Theoretical Chemistry*; Plenum: New York, 1976; Vol. 3.

(27) Hay, P. J.; Wadt, W. R. *J. Chem. Phys.* **1985**, *82*, 270.

(28) Wadt, W. R.; Hay, P. J. *J. Chem. Phys.* **1985**, *82*, 284.

(29) Hay, P. J.; Wadt, W. R. *J. Chem. Phys.* **1985**, *82*, 299.

(30) Cahoon, J. F.; Kling, M. F.; Sawyer, K. R.; Andersen, L. K.; Harris, C. B. *J. Mol. Struct.* **2008**, *890*, 328.

(31) Cahoon, J. F.; Kling, M. F.; Schmatz, S.; Harris, C. B. *J. Am. Chem. Soc.* **2005**, *127*, 12555.

(32) George, M. W.; Dougherty, T. P.; Heilweil, E. J. *J. Phys. Chem.* **1996**, *100*, 201.

(33) Lide, D. R. *CRC Handbook of Chemistry and Physics*; CRC Press: Boca Raton, FL, 2004.

(34) Crabtree, R. H. *Angew. Chem. Int. Ed.* **2003**, *32*, 789.

(35) Brookhart, M.; Green, M. L. H. *J. Organomet. Chem.* **1983**, *250*, 395.

JP107618N